Original Article

Construction and validation of a novel prognostic model using the cellular senescence-associated long non-coding RNA in gastric cancer: a biological analysis

Guoqing Wang[1#], Zhilei Mao[2#], Xiao Zhou[3], Yiming Zou[4], Min Zhao[3]

[1]Department of Gastrointestinal Surgery, the Third Affiliated Hospital of Soochow University, Changzhou First People's Hospital, Soochow University, Changzhou, China; [2]Department of Scientific Research and Education, Changzhou Maternal and Child Health Care Hospital, Changzhou Medical Center, Nanjing Medical University, Changzhou, China; [3]Department of Gastrointestinal Surgery, Changzhou Maternal and Child Health Care Hospital, Changzhou Medical Center, Nanjing Medical University, Changzhou, China; [4]Department of Urinary Surgery, the Third Affiliated Hospital of Soochow University, Changzhou First People's Hospital, Soochow University, Changzhou, China

Contributions: (I) Conception and design: G Wang, M Zhao; (II) Administrative support: M Zhao; (III) Provision of study materials or patients: None; (IV) Collection and assembly of data: Z Mao, X Zhou, Y Zou; (V) Data analysis and interpretation: G Wang, M Zhao; (VI) Manuscript writing: All authors; (VII) Final approval of manuscript: All authors.

[#]These authors contributed equally to this work.

Correspondence to: Min Zhao. Department of Gastrointestinal Surgery, Changzhou Maternal and Child Health Care Hospital, Changzhou Medical Center, Nanjing Medical University, No. 16 Lilac Road, Changzhou 213004, China. Email: zhaomin9601@163.com.

Background: The onset and progression of many cancers, including gastric cancer (GC), are strongly influenced by cell senescence. Numerous studies have demonstrated that long non-coding RNA (lncRNA) impacts cell senescence, thus affecting cancer progression. However, it is not possible to develop a relevant predictive model for GC owing to the absence of a cell senescence-linked lncRNA. Since lncRNAs are linked to cellular senescence, the goal of this work was to create a prognostic signature for stomach adenocarcinoma (STAD) patients utilizing these lncRNAs.

Methods: Through the Pearson correlation, variance, and univariate Cox regression analyses, the cellular senescence lncRNAs that were related to the disease prognosis could be successfully identified. Using the least absolute shrinkage and selection operator (LASSO) regression algorithm, a predictive model that utilized the 11 cellular senescence-linked lncRNAs was constructed. Kaplan-Meier (KM) survival and the receiver operating characteristic (ROC) curve analyses, were employed for assessing the prognostic performance of the proposed model. In addition, ESTIMATE analysis of the low- and high-risk subtypes for the infiltration of various immune cells was carried out. Additionally, the CIBERSORT algorithm was utilized for investigating the infiltration status of numerous immune cells in both groups, while the expression of the immune checkpoint genes in the two groups, was also determined.

Results: In this study, a new prognostic model was constructed using 11 cellular senescence-related lncRNAs. The findings revealed that the OS status of the patients in the low-risk group (category) was significantly higher compared to the high-risk category (P<0.001). The 1-year ROC-area under the curve (AUC) values for the risk score in the training group was 0.714, while the AUC value for the test and comprehensive groups were recorded to be 0.666 and 0.695, respectively, which were obviously due to stage, grade, age, etc. And based on univariate [hazard ratio (HR): 1.435; P<0.001; 95% confidence interval (CI): 1.295–1.589] and multivariate analyses (P<0.001; 95% CI: HR: 1.387; 1.247–1.543), it was noted that risk scores were effectively employed as a patient-independent prognostic factor.

Conclusions: Taken together, these results suggest that cellular senescence-related lncRNAs are likely to be valuable prognostic markers for GC. They also reflect the situation of the STAD immune microenvironment and may provide direction for future GC treatment.

Keywords: Long non-coding RNAs (lncRNAs); cellular senescence; prognostic model; gastric cancer (GC)

Submitted Jun 09, 2022. Accepted for publication Aug 08, 2022.
doi: 10.21037/jgo-22-662
View this article at: https://dx.doi.org/10.21037/jgo-22-662

Introduction

Globally, gastric cancer (GC) was the 5th most prevalent cancer and 3rd major cause of mortality (1). Advances in oncology, such as radiation therapy, neo- and adjuvant chemotherapies, and more recently, immunotherapies, like the immune checkpoint inhibitors (ICIs), are used for treating advanced GC patients; however, in most cases, the prognosis is still poor (2). Therefore, it is essential to determine the significance of the potential biomarkers of GC to improve the prognosis of GC for guiding clinical treatment.

Cellular senescence refers to cells losing their ability to divide so that they are in a permanent state of cell-cycle arrest. Unlike body senescence, cellular senescence can occur at various stages of development and growth and is important for maintaining tissue homeostasis and preventing the expansion of damaged cells. Cellular senescence is linked to several diseases, like neurodegenerative Alzheimer's disease (3), chronic kidney disease (4,5), non-alcoholic fatty liver disease (6), type 2 diabetes (7), and prostate disease in older men (8). However, the link between tumor formation and cellular senescence remains controversial. During the early stages of the senescence-associated secretory phenotype (SASP), SASP refers to the fact that senescent cells are in growth arrest, but still have relatively active metabolic activity, synthesizing a large number of proteins, such as interleukins, growth factors, chemokines, and matrix metalloproteinases. And affects the tissue microenvironment in a paracrine manner, which can promote tissue repair, activate the immune system, and initiate immune surveillance of senescent cells (9). However, prolonged SASP can reshape the microenvironment, leading to chronic inflammation and promoting tumor development. When considering the relationship between cellular senescence and tumors, it is important to systematically study the role of cellular senescence-related genes in GC.

The long non-coding RNAs (lncRNAs) are >200 nucleotides long and can control gene expression, RNA splicing, and microRNA (miRNA) regulation, but do not have protein translation functions. In the past few years, several researchers have noted that the cell senescence-linked lncRNAs were involved in the onset and progression of tumors, including cell senescence-linked *lncRNA-HOXA-AS3* [*HOXA* cluster antisense RNA 3 (*HOXA-AS3*)] through the formation of the *HOXA-AS3* duplex. The formation of more stable *HOXA6* helps in promoting the invasion, proliferation, and migration of malignant lung adenocarcinoma cells (10). *LncRNA-HOTAIR* [HOX transcript antisense RNA (*HOTAIR*)] contributes to cellular senescence and chemoresistance in ovarian and other cancers by reducing *Iκ-Bα* (an *NF-κB* inhibitor) and regulating *NF-κB* activation (11). However, very few researchers have investigated the role played by the cellular senescence-linked lncRNAs in GC. Hence, it is important to identify lncRNAs that are associated with cellular senescence for predicting the prognosis of GC.

Although GC has a considerable number of prognostic markers such as carcinoembryonic antigen (CEA) and cancer antigen 199 (CA199), etc. But the prognosis and survival of GC are not good. Therefore, some new prognostic models have emerged to help clinical judgment and guide clinical treatment [e.g., N6-methyladenosine-related lncRNAs (12), ferroptosis-related lncRNAs (13), and hypoxia-related lncRNAs (14), etc.]. However, there is no research on cellular senescence-related lncRNAs in the stomach adenocarcinoma (STAD) prognostic model. In this research, it was hypothesized that the lncRNAs linked to cellular senescence could be used as promising prognostic biomarkers in the treatment of GC. The relationship between the OS, expression of the cellular senescence-linked lncRNAs, and the clinicopathological factors for STAD patients, was derived using The Cancer Genome Atlas (TCGA) database. Furthermore, a novel prognostic signature integrating 11 lncRNAs linked to cellular senescence was constructed, and its prognostic ability to accurately and independently predict the prognosis of STAD patients was determined. *Figure 1* presents a schematic diagram depicting the workflow used in the study. We present the following article in accordance with the TRIPOD reporting checklist (available at https://jgo.amegroups.com/article/view/10.21037/jgo-22-662/rc).

Methods

Obtaining GC data information from public databases

This study was carried out as per the Declaration of Helsinki

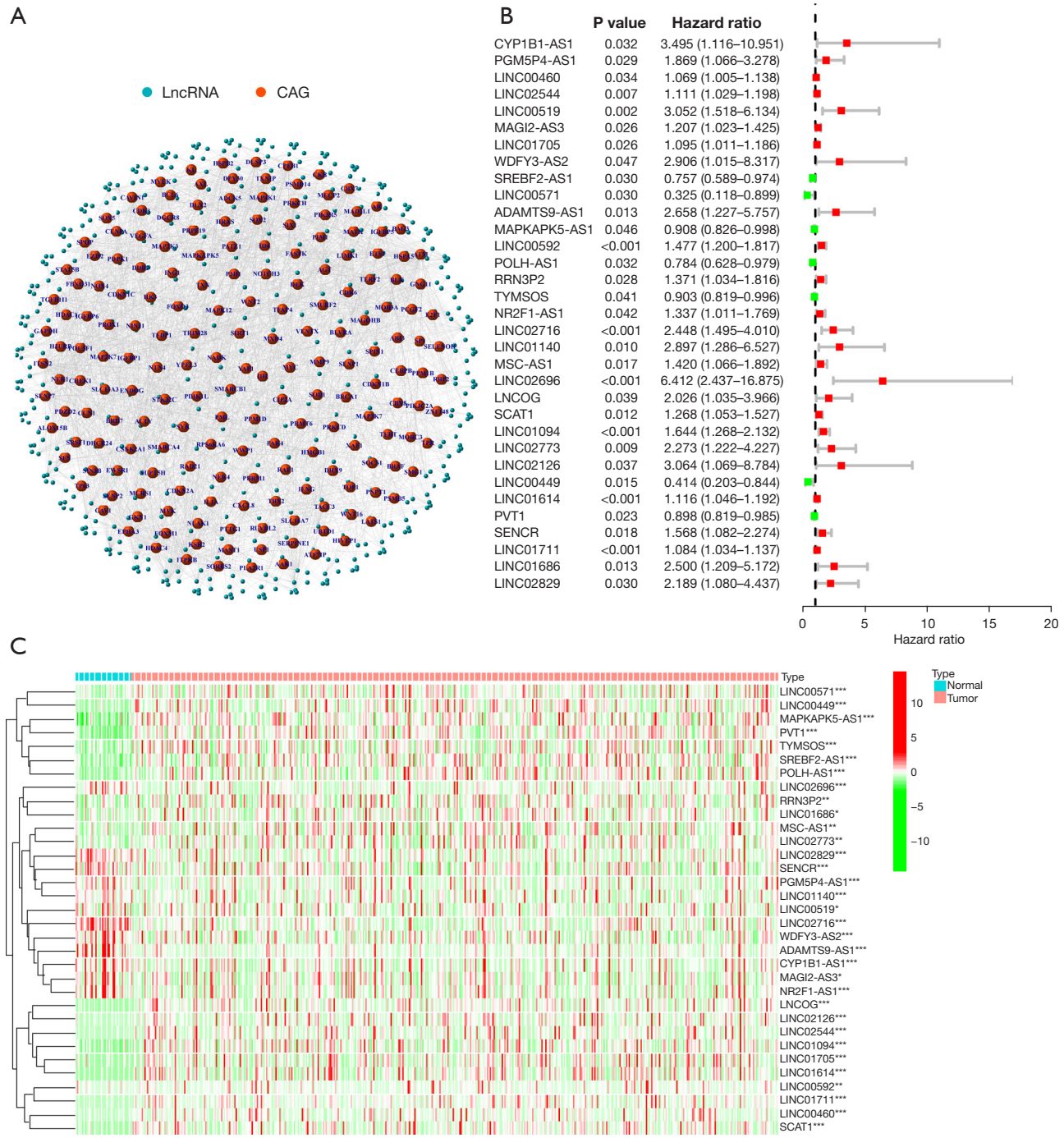

Figure 1 Identification of lncRNAs linked to cellular senescence in GC. (A) Co-expression profile of the lncRNAs and related genes that regulate cellular senescence. (B) Thirty-three cellular senescence lncRNAs were shown to be related to the OS time in GC patients by univariate regression analysis. (C) Heatmap highlighting the differential expression of prognosis-linked lncRNAs associated with cellular senescence. *P<0.05; **P<0.01; ***P<0.001. LncRNAs, long non-coding RNAs; GC, gastric cancer; CAG, cell-aging related genes.

(as revised in 2013). All RNA-seq data [fragments per kilobase million (FPKM) values] and the STAD-related clinical data were acquired from TCGA database (15). This included all information regarding the sex, age, tumor-node-metastasis (TNM) stage, and overall survival (OS) status of GC patients. For differentiating between the lncRNAs and mRNAs, the GTF files were also retrieved from Ensembl (https://uswest.ensembl.org/index.html) for additional analysis (16). The downloaded data were then normalized, processed, and assessed with the help of the R software 4.1.2. A total of 279 cellular senescence-linked genes were derived from the cellular senescence-associated database, i.e., CellAge (https://genomics.senescence.info/cells/) (17), and all the genes were verified experimentally.

Identification of lncRNAs associated with cellular senescence

Using the public database, i.e., CellAge, a total of 279 cellular senescence-linked genes were downloaded and experimentally verified. The detailed gene list is shown in Table S1. The expression data for the 279 cellular senescence-linked genes was further downloaded from the TCGA database. LncRNAs related to cellular senescence genes were detected by Pearson's correlation analysis, and lncRNAs showing a $P<0.001$ and correlation coefficient $|R^2|>0.4$ were screened out. These RNAs are considered to be highly correlated with cellular senescence in GC. Next, a univariate Cox regression analysis was carried out with the above-mentioned cell senescence-linked lncRNAs to screen the lncRNAs linked to the OS of the GC patients. Herein, $P<0.05$ was considered a screening condition.

Constructing and validating the aging-linked lncRNA risk signature

Survival data and expression data were combined, and 371 GC samples were left after excluding samples without any OS status or time. The above 371 GC patients were classified randomly into a test group and a training group in a 1:1 ratio. The best candidates were then examined using least absolute shrinkage and selection operator (LASSO) Cox regression analysis, and prognostic signatures were developed using various cellular senescence lncRNA signatures. The median risk score was employed for separating the low- and high-risk groups (categories). Using the log-rank test and Kaplan-Meier (KM) analysis, differences in the OS across various risk categories in the testing and training datasets were evaluated. The prediction capability of the survival signal was evaluated based on the area under the curve (AUC) values and the time-dependent receiver operating characteristic (ROC) curves. The R packages like caret, pheatmap, survival, and ggpupr were used in the aforementioned procedures.

Correlation between the 11 cellular senescence-linked lncRNA signature models and clinicopathological factors

The Cox regression analysis was implemented for assessing if the prognostic model comprising 11 cellular senescence-linked lncRNAs acted as an independent risk factor for the prognosis of the GC patients. The relationships between the clinical characteristics, molecular subtypes, and prognosis were determined to study the clinical value of molecular subtypes in GC. Age, sex, tumor site, and TNM stage were among the patient's characteristics. The KM technique was employed for identifying the differences in OS status across different groups, and the survminer and survival modules of the R software were used to display the results.

Construction and assessment of the nomogram prediction model

Herein, a nomogram was developed using the risk score and the clinicopathological factors for predicting the 1-, 3-, and 5-year OS outcomes (prognoses) of the patients with GC. This nomogram could be used for assessing the probable clinical significance of the new prognostic model that was developed using the 11 cellular senescence-linked lncRNAs. The consistency between the observed and predicted OS rates by the nomogram was then evaluated using the calibration curves.

Gene set enrichment analysis (GSEA)

The GSEA technique was utilized for determining the associated functions and signaling pathways, whereas the javaGSEA tool was used for identifying the high and low scores of GC patients to determine the differences in the signaling pathways between both risk groups (18). Further investigation was carried out for understanding the biological functions and pathways associated with the differentially expressed genes (DEGs) in both the risk categories. DEGs between the high- and low-risk groups were identified using the cutoff values of false discovery rate (FDR) <0.05 and |log fold change (FC)|>1. The Kyoto

Encyclopedia of Genes and Genomes (KEGG) and Gene Ontology (GO) enrichment analyses were carried out with the Profiler R package cluster (19).

Assessment of the immune microenvironment, infiltration status of immune cells, and the immune surveillance points

The estimation technique of the "estimates" package was used for estimating the proportions of the tumor microenvironment (TME) yielding the immune, stromal, and estimated scores. The proportion of every corresponding component in the TME was seen to increase as the score increased. The activity of the 13 immune-associated pathways was assessed using the single-sample GSEA (ssGSEA) technique, an enrichment technique frequently employed in medical research. The immune infiltration rates of 22 different immunological cells in the tumor samples were determined using the CIBERSORT method. Furthermore, the variations in the Immune Checkpoint genes in both risk groups were determined based on previously published reports (20,21).

Statistical analysis

R soft 4.1.2 was used to process all the data. The correlation between the co-expression of lncRNAs and genes linked to cellular senescence was investigated using Pearson's correlation analysis. Prognostic characteristics were found using LASSO regression analysis. Additionally, the univariate and multivariate Cox analyses were used for evaluating if the risk score could be employed as an independent prognostic factor for STAD. The risk model's sensitivity and specificity were assessed using the Area under the ROC curve. The Fisher's exact or chi-square tests were implemented for probing into the differences across all categorical variables. Furthermore, the Student's *t*-test was used for comparing the normally-distributed continuous variables between both the risk groups.

Results

Identification of lncRNAs associated with cellular senescence

Figure S1 displays the entire process used in this study in detail. TCGA database was utilized to gather the gene expression data of 279 genes linked to cellular senescence in the GC patients, which included 32 normal as well as 375 tumor samples. Pearson's correlation analysis was implemented for identifying the lncRNAs linked to the genes that were related to cellular senescence, and lncRNAs with correlation coefficients $|R^2|>0.4$ and $P<0.001$ were filtered out (*Figure 1A*). $P<0.05$ was the screening threshold, and 33 lncRNAs associated with the OS status of the patients with GC were examined, as presented in *Figure 1B*. *Figure 1C* illustrates the gene expression patterns of lncRNAs in the normal and malignant tissue tumor samples. Subsequently, the expression level of these lncRNAs was examined.

Constructing and validating the prognostic model of cellular senescence-related lncRNAs

Excluding samples without OS status or time, the remaining 371 GC patients were randomly categorized into the test group (n=184) and the training group (n=187) in a 1:1 ratio. LASSO Cox regression analysis was performed based on 33 cellular senescence-associated lncRNAs in the training cohort. It was found that 11 characteristic lncRNAs related to cellular senescence could be used for model construction (*Figure 2A*,*2B*). The risk scores for every patient were estimated using the data for the 11 relevant lncRNAs along with their correlation coefficients based on the formula below:

Risk score = *LINC02544* × 0.011000997 + *LINC00571* × −0.813110635 + *LINC00592* × 0.32778269 + *POLMSH-AS1* × −0.025147195 + *RRN3P2* × 0.221782955 + *TYOS* × −0.023627594 + *LINC02696* × 0.860742118 + *LINC01094* × 0.181390355 + *LINC00449* × −0.027129427 + *LINC01614* × 0.030126879 + *PVT1* × −0.07100812.

The related lncRNAs and their correlation coefficients are shown in *Figure 2C* (the names of these RNAs represent their expression levels). The GC patients included in the training and test groups were further categorized into the low-risk and high-risk categories depending on their median risk scores. *Figure 3A*,*3B* present the risk score, OS status, and gene expression in the GC patients, while *Figure 3C* shows a heatmap of the 11 characteristic genes that were used for constructing the prognostic model.

KM survival curve analysis was employed for assessing the model's prognostic validity in GC patients, and the findings demonstrate that the high-risk category patients showed considerably worse OS rates ($P<0.001$) (*Figure 3D*). Analysis of the ROC curves helped in assessing the model's prediction accuracy. The results revealed that the AUC value in the training group was 0.716 (*Figure 3E*).

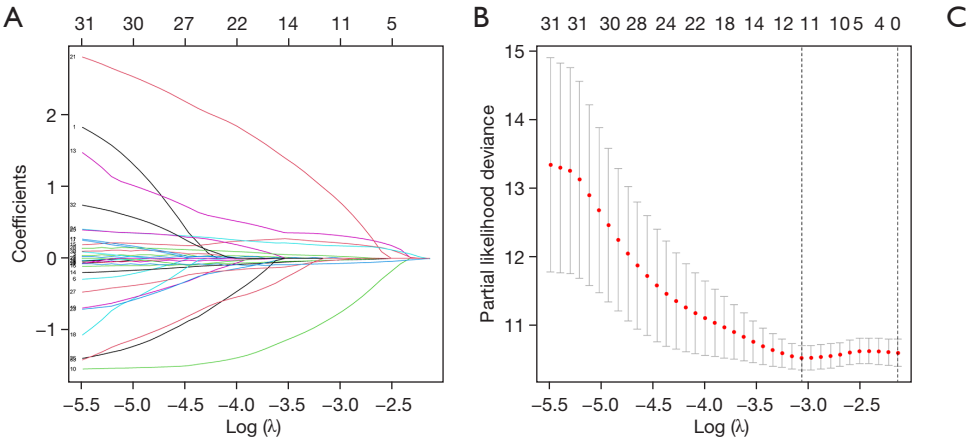

C

Gene	Coef
LINC02544	0.011000997
LINC00571	−0.813110635
LINC00592	0.32778269
POLH-AS1	−0.025147195
RRN3P2	0.221782955
TYMSOS	−0.023627594
LINC02696	0.860742118
LINC01094	0.181390355
LINC00449	−0.027129427
LINC01614	0.030126879
PVT1	−0.07100812

Figure 2 LASSO regression analysis for developing the GC patient risk model, using the cellular senescence-linked lncRNAs. (A) Tuning the parameters for the OS-linked proteins for cross-validating the error curves. Each curve in the figure represents the change trajectory of each independent variable coefficient. (B) Calculating the minimum requirements using imaginary perpendicular lines. (C) The 11 cellular senescence-linked lncRNAs in GC are most closely related to OS rate and the associated risk factors. LASSO, least absolute shrinkage and selection operator; GC, gastric cancer; lncRNAs, long non-coding RNAs; OS, overall survival.

Furthermore, the efficacy and accuracy of the predictions based on the 11 lncRNAs linked to cellular senescence were further verified in the test and combination groups (including all the samples). *Figure 3D* illustrates the results of a KM survival analysis, which showed that the 5-year OS rate in the high-risk GC category was considerably decreased in the verification (P<0.38) and combination groups (P<0.001). The ROC analysis indicated that the AUC values in the test and combination groups were recorded to be 0.666 and 0.695, respectively, as presented in *Figure 3E*. These results show that cellular senescence-related lncRNAs have strong prognostic predictive value.

Correlation between 11 lncRNA signature models associated with cellular senescence and clinicopathological factors

The Cox regression analysis was conducted to determine if the developed prognostic model that was constructed using the 11 cellular senescence-linked lncRNAs can be utilized as the independent risk factor for the GC prognosis. T (P=0.49), age (P=0.01), stage (P<0.001), N (P<0.001), and risk score (P<0.001) were all significant factors that affected the prediction of the GC prognosis, as per the results displayed by the univariate Cox regression results analysis (*Figure 4A*). *Figure 4B* displays the multivariate regression analysis results that indicated that the age [P<0.001; hazard ratio (HR): 1.032; 95% confidence interval (CI): 1.013–1.052] and the risk score (P<0.001; HR: 1.387; 95% CI: 1.247–1.543) were used as the independent prognostic indicators for GC. In addition, *Figure 4C* illustrates the correlation between the clinicopathological factors and the expression profile of the 11 cellular senescence-linked lncRNAs.

For validating the stability of this prognostic model, the GC samples were classified into different categories as per their varying clinical or pathological features. The KM survival analysis was carried out for every subgroup. Results are presented for all the subgroups in terms of factors like age, sex, T stage, N stage, M stage, clinical stage, and grade (*Figure 5A-5N*, respectively). The high-risk groups showed a lower OS rate for all the above factors (except the M stage). These results show the accuracy and stability of the predictive model.

Developing and evaluating a prognostic nomogram depending on the cellular senescence-linked lncRNAs

To assess the potential clinical utility of a prognostic model based on 11 cellular senescence-associated lncRNAs, a nomogram was constructed that determined the likelihood of OS in these patients after adding the scores of many associated factors. The 1-, 3-, and 5-year OS values in the patients with GC were accurately predicted by comparison with ideal prediction models (*Figure 6A,6B*).

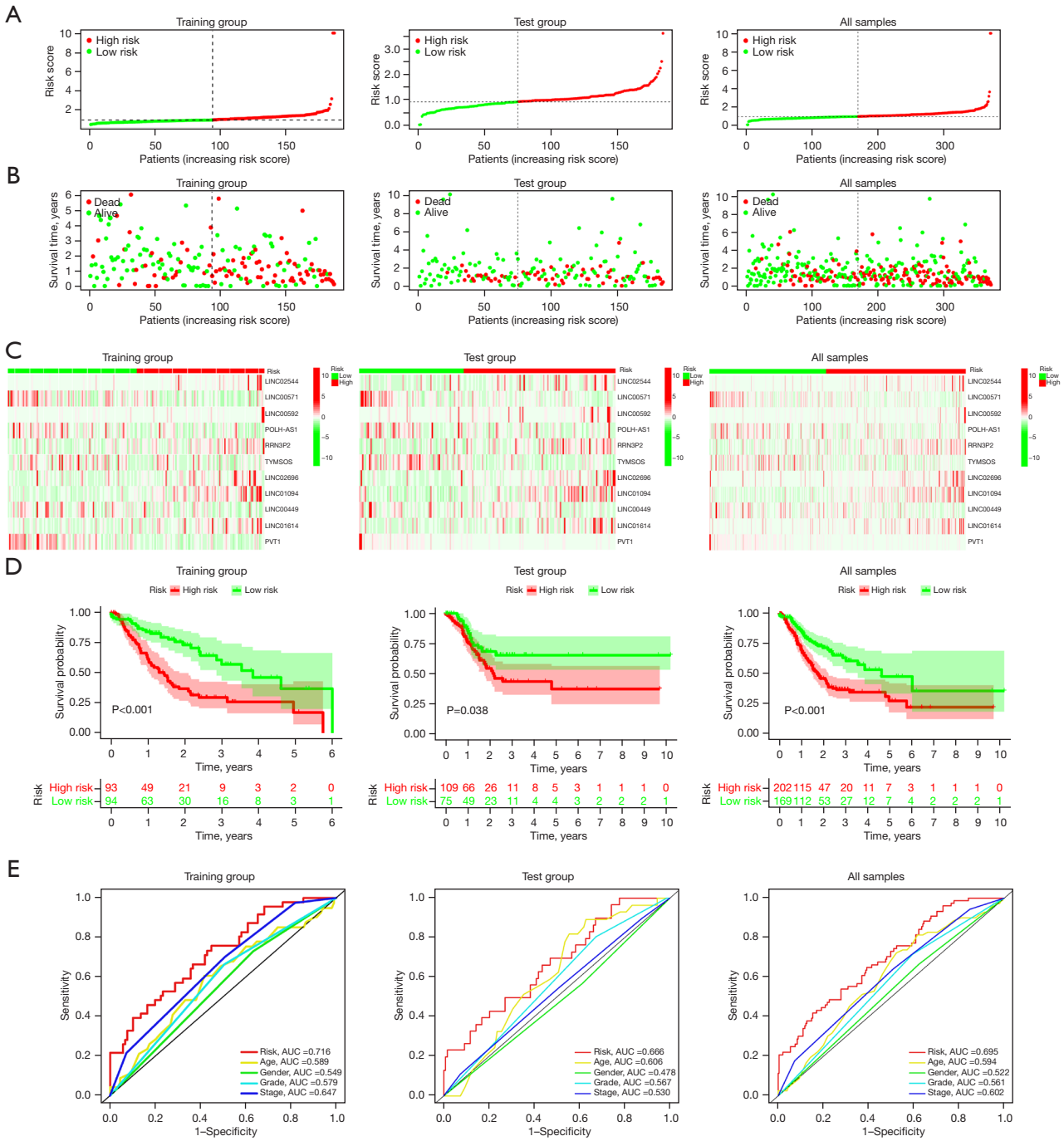

Figure 3 Development and verification of the cellular senescence-linked lncRNA signature models included in the training datasets and the ensemble and validation groups. (A-C) Distribution of the OS status and risk scores, as well as the distribution of the risk scores in the training set, validation set, and overall groups. (D) KM curves for the OS status and survival time among different groups. (E) AUC of the ROC curves that compare the prognostic accuracy of risk scores and a few other predictive parameters used in the training set, validation, and overall groups. AUC, area under the curve; lncRNAs, long non-coding RNAs; OS, overall survival; KM, Kaplan-Meier; ROC, receiver operating characteristics.

Figure 4 Analysis of the correlation between various clinicopathological characteristics and prognostic variables in the TCGA cohort. (A,B) Risk score and other clinical parameters related to GC were investigated using the univariate and multivariate Cox regression analyses. (C) Heatmap for the clinical correlation. Green denotes a low-risk subtype, whereas red denotes a high-risk category. The main abscissa shows the high-risk group and low-risk group; we show the high-risk category in red and the low-risk subtype in blue. The tumor TNM stage, gender, age, survival time, OS status, and the clinicopathological stage are also included in the abscissa stratification; the ordinate shows the expression levels of distinctive prognostic lncRNAs linked to ferroptosis in all samples. *P<0.05; **P<0.01. TCGA, The Cancer Genome Atlas; GC, gastric cancer; TNM, tumor-node-metastasis; OS, overall survival; lncRNAs, long non-coding RNAs.

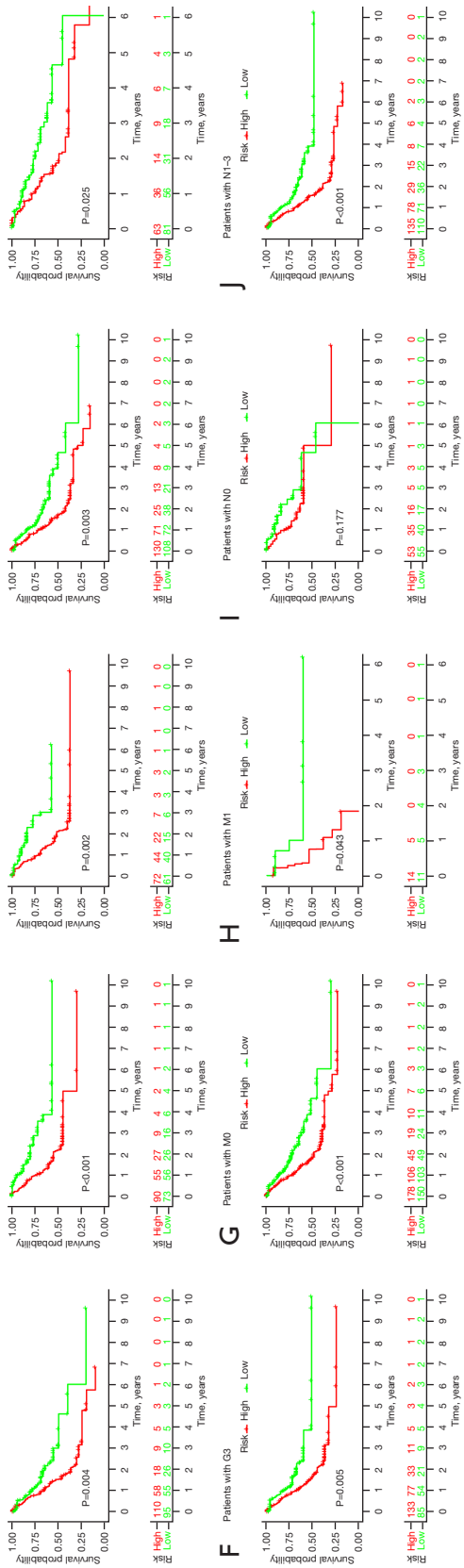

Figure 5 KM analysis shows the OS status curves of the patients with GC in different subgroups. (A) Age >65; (B) age ≤65; (C) females; (D) males; (E) G1–G2; (F) G3; (G) M0; (H) M1; (I) N0; (J) N1–N3; (K) stage I + II; (L) stage III + IV; (M) T1–T2; (N) T3–T4. KM, Kaplan-Meier; OS, overall survival; GC, gastric cancer.

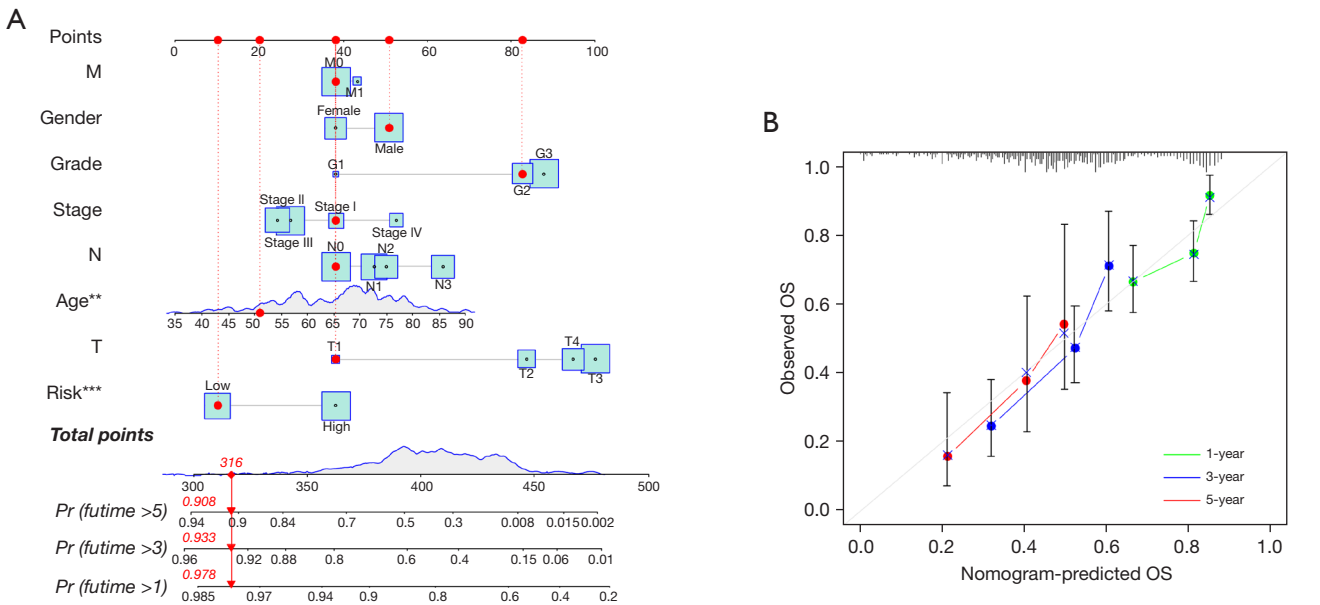

Figure 6 A new nomogram is constructed for predicting the OS status in patients with GC. (A) Nomogram of the clinicopathological variables and the predictive model integrating 11 lncRNAs linked to cellular senescence. (B) The calibration curves were employed for assessing the accuracy of the nomogram model. The ideal nomogram is represented by the gray diagonal dashed line. **P<0.01; ***P<0.001. OS, overall survival; GC, gastric cancer; lncRNAs, long non-coding RNAs.

Molecular function (MF) and pathway discovery by GSEA, GO, and KEGG analyses

To investigate the pathway differences between different groups of 11 cellular senescence-related lncRNAs, the GSEA technique was implemented. The results indicated that many pathways associated with tumor progression were enriched significantly in the high-risk category, like *JAK-STAT* and *MAPK* signaling pathways. Additionally, the patients in the high-risk category showed significant enrichment in the immune-related pathways, like the B-cell and T-cell receptor-related pathways, NK-cell-mediated cytotoxicity-based pathways, and the gut immune network-linked pathways. Significant enrichment of high-risk groups was found in many tumors and immune-related diseases, such as autoimmune-related diseases, melanoma, basal cell carcinoma, and renal cell carcinoma, as shown in *Figure* 7. Table S2 presents additional details. The low-risk patients had similar genes that were primarily enriched in the DNA repair-associated pathways and pyrimidine metabolism-related pathways, as shown in *Figure* 7. Table S3 presents additional details. The functional and pathway enrichment analyses associated with 2 sets of DEGs were conducted. Cutoff thresholds for |logFC|>1 and FDR <0.05 followed by the annotated KEGG and GO enrichment analyses (P<0.05), were utilized to identify the DEGs between both the risk groups. Similar to the GSEA findings, KEGG analysis revealed a high enrichment of numerous immune-related pathways (*Figure 7B*). A GO analysis was carried out and the findings revealed that MF, biological process (BP), and cellular component (CC) were subjected to enrichment. In *Figure 7C*, the outcomes of the above 3 analyses were displayed. Taken together, all the findings suggested that the risk scores for 11 cellular senescence-associated lncRNA signatures are primarily involved in tumor development and are associated with tumor immunity.

Association of cellular senescence-associated lncRNAs with the infiltration of the immune cells and different immune checkpoints

Using the ESTIMATE algorithm, the immune, stromal, and ESTIMATE scores of the 2 risk groups were predicted. As presented in *Figure 8A-8C*, some differences were noted in the immune (P<0.001), stromal (P<0.001), and ESTIMATE (P<0.001) scores across the groups. In comparison to high-risk patients, the low-risk patients showed a higher tumor purity. The ssGSEA-based correlation analysis was carried out between different

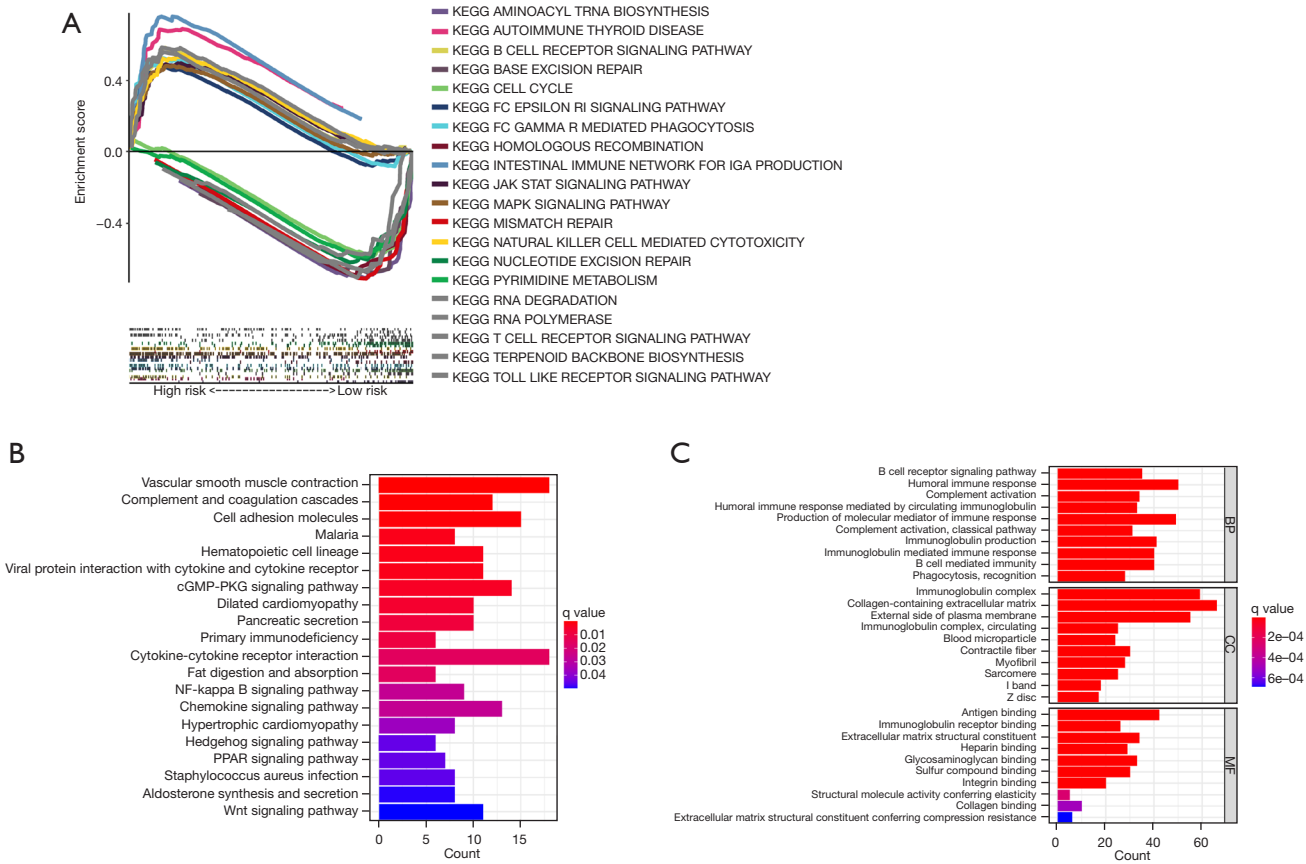

Figure 7 Biological functions and the pathway enrichment analyses of the high- and low-risk categories depending on the prognostic markers of cellular senescence-linked lncRNAs. (A) GSEA reveals enriched pathways in high and low groups. (B) KEGG analysis reveals enrichment of multiple pathways involved in the immune system and cancer proliferation. (C) GO analysis reveals significant enrichment of immune-related biologic processes. KEGG, Kyoto Encyclopedia of Genes and Genomes; BP, biological process; CC, cellular component; MF, molecular function; lncRNAs, long non-coding RNAs; GSEA, gene set enrichment analysis; GO, Gene Ontology.

immune cell subsets and the associated functions and the findings revealed substantial differences in the immune functions across the groups. Immune cell functions such as type I interferon (IFN) response, inflammation-promoting, type II IFN response, T cell co-stimulation, antigen presenting cell (APC) co-inhibition, cytolytic activity, checkpoint, T cell co-inhibition, human leukocyte antigen (HLA), para-inflammation, APC co-stimulation, and CC chemokine receptor (CCR), were increased significantly ($P<0.001$) in the high-risk group (*Figure 8D*). Correlation analyses among the 22 immune cells revealed differences in 4 cell types, including resting dendritic cells, monocytes, M2 macrophages, and plasma cells. Plasma cells were observed to be prevalent in the patients included in the low-risk category, whereas the high-group patients showed a higher prevalence of the other three cell types (*Figure 8E*). The results also showed that blocking the immune checkpoint pathways could be a very promising strategy for achieving anticancer immunity. As a result, the variations in the expression of multiple ICGs were assessed and compared between both groups. Nearly all the immune checkpoints were different between both groups. According to the findings (*Figure 9*), the immune-linked genes were more prevalent in the high-risk category, suggesting that ICIs are more responsive in the patients included in the high-risk category, who were receiving immunotherapy.

Discussion

Many current reports have focused on determining the role played by the cellular senescence-linked genes in tumors. Recently, lncRNAs related to cellular senescence have

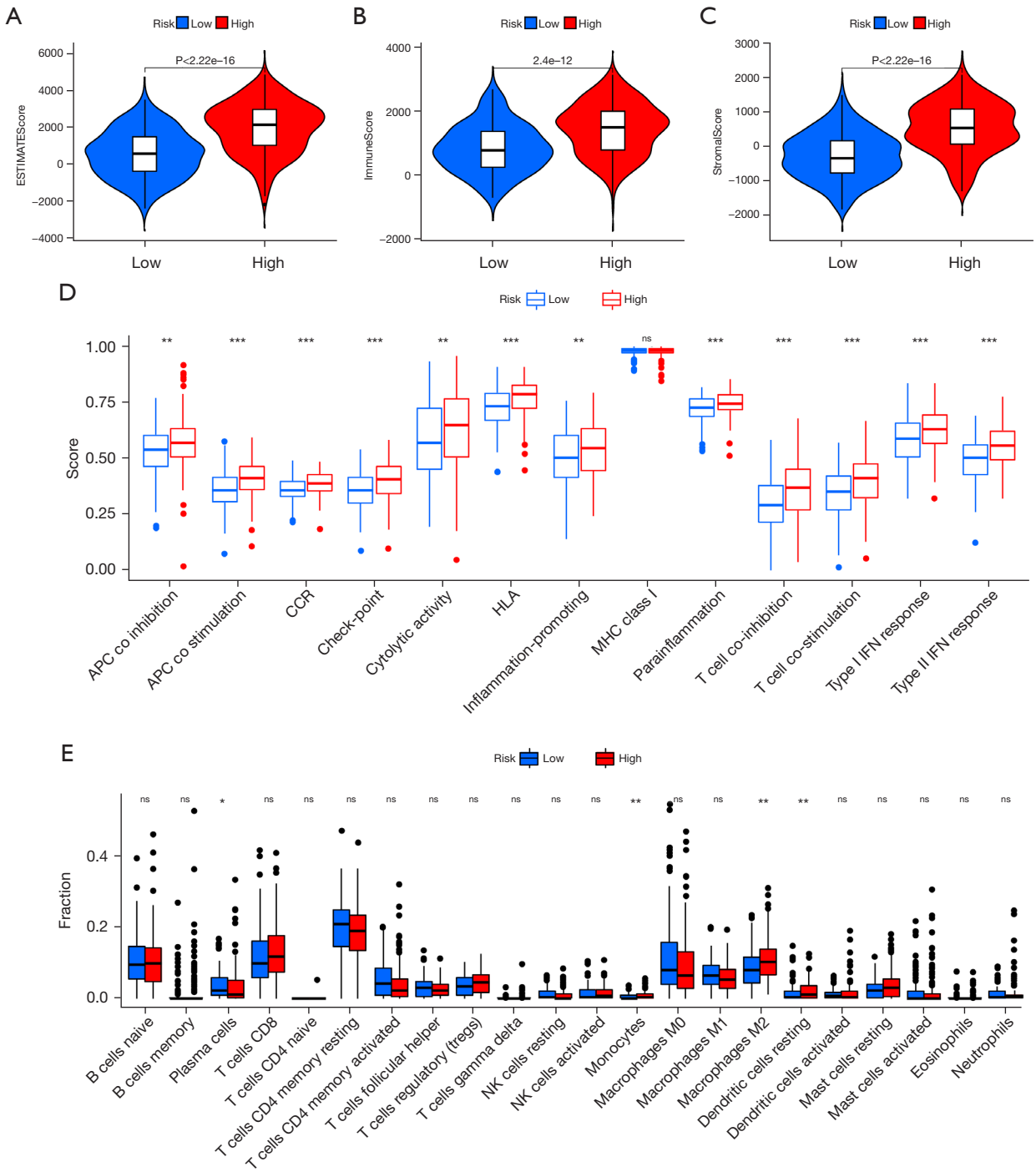

Figure 8 Analysis of the infiltration landscape of the different immune cells in the GC patients. (A) Estimated, (B) immune, and (C) stromal scores for the GC patients in both the risk categories. (D) In the TCGA dataset, 13 immune-linked functions were compared between the 2 different risk groups. (E) Box plot for analyzing the 22 immune cells in the patients with colon cancer in both the risk groups. *P<0.05; **P<0.01; ***P<0.001; ns, not significant. GC, gastric cancer; TCGA, The Cancer Genome Atlas.

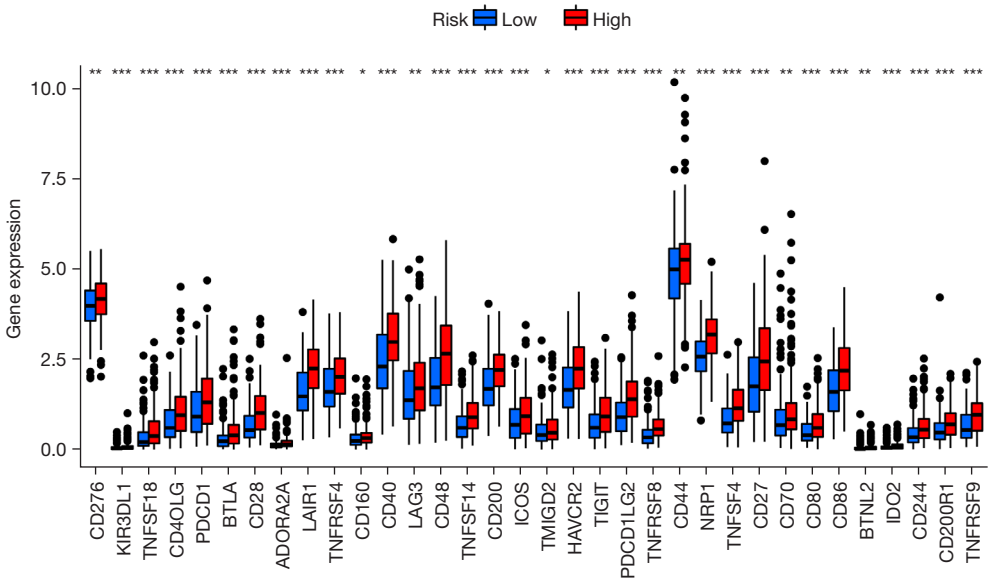

Figure 9 Gene expression of the different immune checkpoint genes between both the risk groups. *P<0.05; **P<0.01; ***P<0.001.

attracted more and more attention. For example, Si *et al.* reported that lncRNA-HEIH promoted ovarian cancer cell proliferation by suppressing cellular senescence through the *miR-3619-5p/CTTNBP2* axis (22). Li *et al.* found that the lncRNA USP2-AS1 acts as a direct transcriptional target of c-Myc to inhibit senescence and promote tumor progression (23). Hence, it is essential to identify potential markers of cellular senescence-related lncRNAs in cancer. However, the current research in GC is still insufficient.

In this research, the expression profiles of 279 cellular senescence-linked genes were analyzed, and they were observed to be updated by the CellAge database and validated experimentally. Depending on the co-expression of the cellular senescence-linked genes, the related lncRNAs were then screened. Next, the expression profiles of the senescence-linked lncRNAs and the prognosis of the patients with GC were downloaded using the TCGA cohort and then examined. In total, 33 prognostic lncRNAs were identified using these results. The best candidates were further analyzed using the LASSO Cox regression analysis for constructing the novel prognostic model integrating 11 cellular senescence-linked lncRNAs. This novel model was verified using the internal cohort. Additionally, a predictive nomogram was constructed after combining the clinical traits with the lncRNA markers related to cellular senescence. The design of the new signature could help in differentiating among the different risk samples. The OS status of the STAD in the training cohort was lower in the high-risk category in comparison to that in the low-risk subtype, and similar findings were observed in the test cohort. Furthermore, the risk scores were found to be the independent predictor of OS in STAD patients, depending on the findings of the univariate and multivariate Cox regression analyses. Altogether, these findings show how the prognostic signatures integrating cellular senescence-linked lncRNAs could successfully predict the OS rate in GC patients.

The TME is crucial for the advancement of malignant tumors, immune evasion, and treatment resistance. TME can be impacted by variations in any gene. Therefore, in this report, the correlation noted between the infiltration status of immune cells in the tumor tissues and the cellular senescence-linked lncRNAs was examined.

Tumor-associated macrophages have been extensively studied, and their numbers are thought to correlate with tumor grade and survival (24,25). Although the function of tumor-associated macrophages is highly plastic, tumor-associated macrophages eventually transition to an immunosuppressive phenotype as the tumor progresses. As characteristic surface molecules of tumor-associated macrophages, CD163 and CD206 have properties related to stimulating angiogenesis, inhibiting adaptive immunity, and promoting tumor growth and metastasis (26-28). The predominant phenotype of tumor-associated macrophages is currently considered to be the M2 type. Some studies have found that lung cancer cells can induce

the polarization of macrophages to the M2 subtype, which in turn enhances the invasion, migration, and epithelial-mesenchymal transition (EMT) of lung cancer cells (29,30). Yamaguchi *et al.* reported that M2 macrophages promote peritoneal dissemination in GC patients and lead to tumor spread and progression (31). The M2 isoform promotes EMT in pancreatic cancer cells through the *TLR-4/IL-10* signaling pathway (32). M2 macrophages are considered tumor-promoting "bad" macrophages because they produce growth factors, activate tissue repair and angiogenesis, and have high scavenging activity that suppresses adaptive immune responses (33). These results are consistent with those observed in this study, where the levels of M2 macrophages were seen to be significantly enhanced in the high-risk category compared to the low-risk category. Macrophages are derived from monocytes. The study found that after monocytes reach the tumor after the Notch signaling transcriptional regulator *RBPJ* is activated, they differentiate into tumor-associated macrophages (34). This finding is also consistent with the findings reported in this study, and the enrichment analysis showed significant enrichment in the Notch pathway. Immune cell analysis also indicated that the GC patients in the high-risk category showed a higher level of monocytes compared to the low-risk GC patients. Therefore, the high-risk category was significantly associated with immunity in the TME and likely contributed to the progression of GC by increasing the infiltration level of M2-type macrophages. Immune checkpoints include immunostimulatory factors and immunosuppressive molecules. In recent years, ICIs represented by the *PD-1/PD-L1* antibodies were commonly used in tumors. Moreover, the variations noted in the gene expression of immune checkpoint genes between both the categories were assessed, and the results revealed that the GC patients in the high-risk category showed a higher level of immune-related genes, indicating that ICIs are more sensitive in high-risk GC patients receiving immunotherapy.

This study has a few drawbacks. Firstly, the TCGA database was used as the sole data source in this study, with no additional datasets used to verify our findings. Other datasets should be used in future studies to confirm the performance of the proposed predictive signature. Secondly, the results noted in the study need to be validated, both *in vivo* and *in vitro*. The underlying processes of the cellular senescence-linked lncRNAs were not studied. Therefore, to assess the predictive performance of the constructed signature and identify the relevant regulatory mechanisms, functional studies should explore these 11 lncRNAs separately and thoroughly. Despite all these drawbacks, this is, to the best of the researcher's knowledge, the first report where the cellular senescence-linked lncRNAs have been established and validated in a GC prognostic model.

Conclusions

According to the findings presented in this study, the cellular senescence-linked lncRNA signatures can act as an effective prognostic marker in GC patients. It will direct the development of the GC biomarkers and a more precise immune modulation.

Acknowledgments

Funding: This work was supported by the Application Foundation Project of Changzhou Science and Technology Bureau (No. CJ20210165) and the General Project of Nanjing Medical University (No. NMUB2020073).

Footnote

Reporting Checklist: The authors have completed the TRIPOD reporting checklist. Available at https://jgo.amegroups.com/article/view/10.21037/jgo-22-662/rc

Conflicts of Interest: All authors have completed the ICMJE uniform disclosure form (available at https://jgo.amegroups.com/article/view/10.21037/jgo-22-662/coif). The authors have no conflicts of interest to declare.

Ethical Statement: The authors are accountable for all aspects of the work in ensuring that questions related to the accuracy or integrity of any part of the work are appropriately investigated and resolved. The study was conducted in accordance with the Declaration of Helsinki (as revised in 2013).

References

1. Li Y, Yan J, Wang Y, et al. LINC00240 promotes gastric cancer cell proliferation, migration and EMT via the miR-124-3p / DNMT3B axis. Cell Biochem Funct 2020;38:1079-88.
2. Kwak Y, Seo AN, Lee HE, et al. Tumor immune response and immunotherapy in gastric cancer. J Pathol Transl Med 2020;54:20-33.
3. Kritsilis M, V Rizou S, Koutsoudaki PN, et al. Ageing, Cellular Senescence and Neurodegenerative Disease. Int J Mol Sci 2018;19:2937.
4. Wang Y, Wang Y, Yang M, et al. Implication of cellular senescence in the progression of chronic kidney disease and the treatment potencies. Biomed Pharmacother 2021;135:111191.
5. Tan H, Xu J, Liu Y. Ageing, cellular senescence and chronic kidney disease: experimental evidence. Curr Opin Nephrol Hypertens 2022;31:235-43.
6. Engelmann C, Tacke F. The Potential Role of Cellular Senescence in Non-Alcoholic Fatty Liver Disease. Int J Mol Sci 2022;23:652.
7. Narasimhan A, Flores RR, Robbins PD, et al. Role of Cellular Senescence in Type II Diabetes. Endocrinology 2021;162:bqab136.
8. Fiard G, Stavrinides V, Chambers ES, et al. Cellular senescence as a possible link between prostate diseases of the ageing male. Nat Rev Urol 2021;18:597-610.
9. Zhang JW, Zhang D, Yu BP. Senescent cells in cancer therapy: why and how to remove them. Cancer Lett 2021;520:68-79.
10. Zhang H, Liu Y, Yan L, et al. Increased levels of the long noncoding RNA, HOXA-AS3, promote proliferation of A549 cells. Cell Death Dis 2018;9:707.
11. Özeş AR, Miller DF, Özeş ON, et al. NF-κB-HOTAIR axis links DNA damage response, chemoresistance and cellular senescence in ovarian cancer. Oncogene 2016;35:5350-61.
12. Xu S, Chen W, Wang Y, et al. N6-methyladenosine-related lncRNAs identified as potential biomarkers for predicting the overall survival of Asian gastric cancer patients. BMC Cancer 2022;22:721.
13. Li J, Xiang R, Song W, et al. A Novel Ferroptosis-Related LncRNA Pair Prognostic Signature Predicts Immune Landscapes and Treatment Responses for Gastric Cancer Patients. Front Genet 2022;13:899419.
14. Fan Z, Wang Y, Niu R. Identification of the three subtypes and the prognostic characteristics of stomach adenocarcinoma: analysis of the hypoxia-related long non-coding RNAs. Funct Integr Genomics 2022. [Epub ahead of print]. doi: 10.1007/s10142-022-00867-3.
15. Hutter C, Zenklusen JC. The Cancer Genome Atlas: Creating Lasting Value beyond Its Data. Cell 2018;173:283-5.
16. Howe KL, Achuthan P, Allen J, et al. Ensembl 2021. Nucleic Acids Res 2021;49:D884-91.
17. Basisty N, Kale A, Jeon OH, et al. A proteomic atlas of senescence-associated secretomes for aging biomarker development. PLoS Biol 2020;18:e3000599.
18. Subramanian A, Tamayo P, Mootha VK, et al. Gene set enrichment analysis: a knowledge-based approach for interpreting genome-wide expression profiles. Proc Natl Acad Sci U S A 2005;102:15545-50.
19. Yu G, Wang LG, Han Y, et al. clusterProfiler: an R package for comparing biological themes among gene clusters. OMICS 2012;16:284-7.
20. Newman AM, Liu CL, Green MR, et al. Robust enumeration of cell subsets from tissue expression profiles. Nat Methods 2015;12:453-7.
21. Zhang Y, Zheng J. Functions of Immune Checkpoint Molecules Beyond Immune Evasion. Adv Exp Med Biol 2020;1248:201-26.
22. Si L, Chen J, Yang S, et al. lncRNA HEIH accelerates cell proliferation and inhibits cell senescence by targeting miR-3619-5p/CTTNBP2 axis in ovarian cancer. Menopause 2020;27:1302-14.
23. Li B, Zhang G, Wang Z, et al. c-Myc-activated USP2-AS1 suppresses senescence and promotes tumor progression via stabilization of E2F1 mRNA. Cell Death Dis 2021;12:1006.
24. Tiainen S, Tumelius R, Rilla K, et al. High numbers of macrophages, especially M2-like (CD163-positive), correlate with hyaluronan accumulation and poor outcome in breast cancer. Histopathology 2015;66:873-83.
25. Gartrell RD, Marks DK, Hart TD, et al. Quantitative Analysis of Immune Infiltrates in Primary Melanoma. Cancer Immunol Res 2018;6:481-93.
26. Ino Y, Yamazaki-Itoh R, Shimada K, et al. Immune cell infiltration as an indicator of the immune microenvironment of pancreatic cancer. Br J Cancer 2013;108:914-23.
27. Di Caro G, Cortese N, Castino GF, et al. Dual prognostic significance of tumour-associated macrophages in human pancreatic adenocarcinoma treated or untreated with chemotherapy. Gut 2016;65:1710-20.
28. Noy R, Pollard JW. Tumor-associated macrophages: from mechanisms to therapy. Immunity 2014;41:49-61.

29. Guo Z, Song J, Hao J, et al. M2 macrophages promote NSCLC metastasis by upregulating CRYAB. Cell Death Dis 2019;10:377.
30. Yu X, Xu M, Li N, et al. β-elemene inhibits tumor-promoting effect of M2 macrophages in lung cancer. Biochem Biophys Res Commun 2017;490:514-20.
31. Yamaguchi T, Fushida S, Yamamoto Y, et al. Tumor-associated macrophages of the M2 phenotype contribute to progression in gastric cancer with peritoneal dissemination. Gastric Cancer 2016;19:1052-65.
32. Liu CY, Xu JY, Shi XY, et al. M2-polarized tumor-associated macrophages promoted epithelial-mesenchymal transition in pancreatic cancer cells, partially through TLR4/IL-10 signaling pathway. Lab Invest 2013;93:844-54.
33. Tariq M, Zhang J, Liang G, et al. Macrophage Polarization: Anti-Cancer Strategies to Target Tumor-Associated Macrophage in Breast Cancer. J Cell Biochem 2017;118:2484-501.
34. Franklin RA, Liao W, Sarkar A, et al. The cellular and molecular origin of tumor-associated macrophages. Science 2014;344:921-5.

(English Language Editor: R. Scott)

Cite this article as: Wang G, Mao Z, Zhou X, Zou Y, Zhao M. Construction and validation of a novel prognostic model using the cellular senescence-associated long noncoding RNA in gastric cancer: a biological analysis. J Gastrointest Oncol 2022;13(4):1640-1655. doi: 10.21037/jgo-22-662

Table S1 List of genes that were related to cellular senescence

MARCHF5
AAK1
ABI3
ACLY
ADCK5
AGT
AKR1B1
AKT1
ALOX15B
AR
ARPC1B
ASF1A
ASPH
ATF7IP
ATM
AURKA
AXL
BAG3
BCL6
BHLHE40
BLK
BLVRA
BMI1
BRAF
BRCA1
BRD7
BTG3
SELENOH
CAV1
CBX7
CBX8
CCND1
CDK1
CDK18
CDK2AP1
CDK4
CDK6
CDKN1A
CDKN1B
CDKN1C
CDKN2A
CDKN2B
CEBPB
CENPA
CHEK1
CKB
CPEB1
CSNK1A1
CSNK2A1
CXCL1
CCN1
DDB2
DEK
DGCR8
DHCR24
DHX9
DLX2
DPY30
DUSP16
DUSP3
E2F1
EHF
ENDOG
EPHA3
ERRFI1
ETS1
ETS2
EWSR1
EZH2
FASTK
FBXO31
FOS
FOXM1
FOXO3
FXR1
G6PD
GAPDH
GATA4
GKN1
GLB1
GNG11
GRK6
HDAC1
HDAC4
HIVEP1
HJURP
HK3
HMGB1
HRAS
HSPA5
HSPB2
ID1
ID4
IFNG
IGFBP1
IGFBP3
IGFBP5
IGFBP6
IL1A
CXCL8
ING1
ING2
IRF3
IRF5
IRF7
ITGB4
ITPK1
ITPKB
ITSN2
KCNJ12
KDM4A
KDM5B
CIP2A
KL
KSR2
LATS1
LEO1
LGALS3
LIMA1
LIMK1
MAD2L1
MAGEA2
MAGOH
MAGOHB
MAP2K1
MAP2K2
MAP2K3
MAP2K6
MAP2K7
MAP3K6
MAP3K7
MAP4K1
MAPK12
MAPK14
MAST1
MATK
MCL1
MCRS1
MDH1
MECP2
MMP9
MOB3A
MORC3
MORF4
MVK
MXD4
MYC
MYLK
NADK
NANOG
NDRG1
NEK1
NEK4
NEK6
NFE2L2
NINJ1
NOTCH3
NOX4
NR2E1
NTN4
NUAK1
OTX2
P3H1
PAK4
PATZ1
PBRM1
PCGF2
PDCD10
PDIK1L
PDPK1
PDZD2
PEBP1
PEX19
PIAS4
PIK3C2A
PIK3R5
PIM1
PKM
PLA2R1
PML
PMVK
PNPT1
POT1
POU5F1
PPM1B
PPM1D
PRKCD
PRKCH
PRMT6
PROX1
PRPF19
PSMB5
PSMD14
CAVIN1
PTTG1
RAD21
RAF1
RB1
RBP2
RBX1
RNASEL
RPS6KA6
RSL1D1
RUNX1
RUVBL2
SENP1
SENP2
SENP7
SERPINE1
SFN
SGK1
SIK1
SIN3B
SIRT1
SIRT6
SIX1
SLC13A3
SLC16A7
SMG1
SMURF2
SNAI1
SOCS1
SOD1
SORBS2
SOX2
SOX5
SP1
SPIN1
SPOP
SRC
SREBF1
SRSF1
STAT5B
STK32C
STK40
SUPT5H
SYK
TACC3
TBX2
TERC
TERF2
TERT
TFAP4
TFDP1
TGFB1I1
TLR3
TMSB4X
TNFSF13
TNFSF15
TOP1
TP53
TP63
TPR
TRIM28
TRPM8
TXN
TXNIP
TYK2
UBTD1
USP1
VEGFA
VENTX
WNT16
WNT2
WRN
WT1
WWP1
XAF1
YAP1
YPEL3
ZFP36
ZMAT3
ZNF148

https://dx.doi.org/10.21037/jgo-22-662

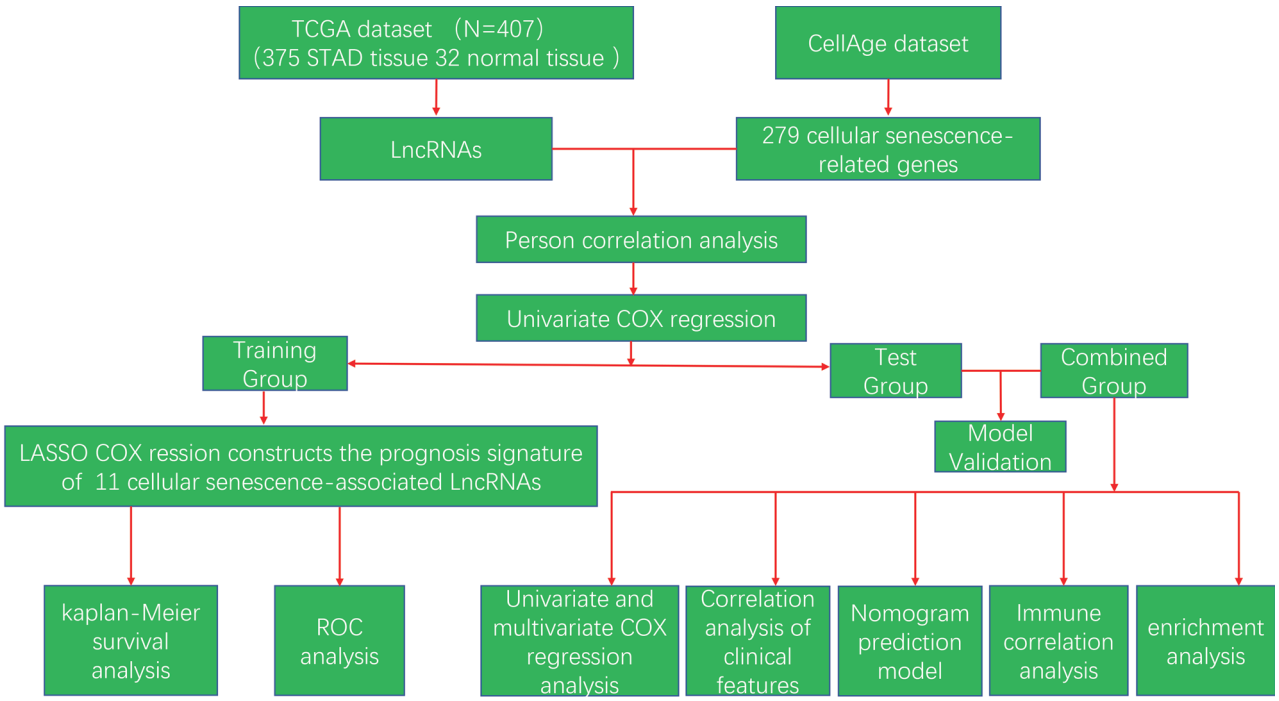

Figure S1 The detailed process of this analysis. TCGA, The Cancer Genome Atlas; STAD, stomach adenocarcinoma; lncRNAs, long non-coding RNAs; LASSO, least absolute shrinkage and selection operator; ROC, receiver operating characteristic.

https://dx.doi.org/10.21037/jgo-22-662

Table S2 Through GSEA enrichment analysis, Screening of classical pathways enriched in high-risk groups

Pathway	Size	ES	NES	NOM P value	FDR q value	Leading edge
KEGG_TOLL_LIKE_RECEPTOR_SIGNALING_PATHWAY	102	0.58	2.11	0.004	0.002	Tags =34%, list =12%, signal =39%
KEGG_INTESTINAL_IMMUNE_NETWORK_FOR_IGA_PRODUCTION	46	0.76	2.05	0.002	0.004	Tags =63%, list =11%, signal =71%
KEGG_AUTOIMMUNE_THYROID_DISEASE	50	0.69	2.02	0.002	0.006	Tags =50%, list =19%, signal =62%
KEGG_NATURAL_KILLER_CELL_MEDIATED_CYTOTOXICITY	132	0.54	1.95	0.006	0.01	Tags =43%, list =18%, signal =53%
KEGG_JAK_STAT_SIGNALING_PATHWAY	155	0.5	1.92	0.002	0.013	Tags =37%, list =18%, signal =45%
KEGG_MAPK_SIGNALING_PATHWAY	267	0.48	1.92	0	0.013	Tags =30%, list =13%, signal =34%
KEGG_RENAL_CELL_CARCINOMA	70	0.55	1.88	0.004	0.016	Tags =39%, list =16%, signal =46%
KEGG_T_CELL_RECEPTOR_SIGNALING_PATHWAY	108	0.56	1.87	0.006	0.017	Tags =37%, list =12%, signal =42%
KEGG_B_CELL_RECEPTOR_SIGNALING_PATHWAY	75	0.59	1.8	0.02	0.027	Tags =43%, list =13%, signal =49%
KEGG_FC_GAMMA_R_MEDIATED_PHAGOCYTOSIS	96	0.52	1.79	0.01	0.029	Tags =34%, list =12%, signal =39%
KEGG_MELANOMA	71	0.5	1.77	0.008	0.033	Tags =30%, list =12%, signal =33%
KEGG_BASAL_CELL_CARCINOMA	55	0.54	1.76	0.013	0.033	Tags =29%, list =7%, signal =31%
KEGG_FC_EPSILON_RI_SIGNALING_PATHWAY	79	0.48	1.75	0.004	0.034	Tags =30%, list =12%, signal =34%

GSEA, gene set enrichment analysis; KEGG, Kyoto Encyclopedia of Genes and Genomes; ES, enrichment score; NES, normalized enrichment score; NOM, nominal; FDR, false discovery rate.

Table S3 GSEA enrichment analysis for screening the enriched classical pathways in the low-risk groups

Pathway	Size	ES	NES	NOM P value	FDR q value	Leading edge
KEGG_SPLICEOSOME	127	−0.71	−2.15	0.002	0.006	Tags =72%, list =19%, signal =88%
KEGG_PYRIMIDINE_METABOLISM	98	−0.6	−2.02	0.002	0.015	Tags =58%, list =16%, signal =69%
KEGG_RNA_POLYMERASE	29	−0.7	−1.98	0.002	0.02	Tags =62%, list =16%, signal =74%
KEGG_BASE_EXCISION_REPAIR	35	−0.7	−1.98	0.006	0.017	Tags =57%, list =15%, signal =67%
KEGG_HOMOLOGOUS_RECOMBINATION	28	−0.72	−1.95	0.004	0.019	Tags =71%, list =20%, signal =89%
KEGG_DNA_REPLICATION	36	−0.78	−1.92	0.004	0.022	Tags =89%, list =19%, signal =110%
KEGG_AMINOACYL_TRNA_BIOSYNTHESIS	41	−0.72	−1.89	0.002	0.028	Tags =71%, list =17%, signal =85%
KEGG_CELL_CYCLE	125	−0.59	−1.89	0.014	0.026	Tags =53%, list =14%, signal =61%
KEGG_MISMATCH_REPAIR	23	−0.74	−1.83	0.01	0.039	Tags =78%, list =16%, signal =93%
KEGG_TERPENOID_BACKBONE_BIOSYNTHESIS	15	−0.75	−1.82	0.002	0.038	Tags =80%, list =20%, signal =99%
KEGG_NUCLEOTIDE_EXCISION_REPAIR	44	−0.63	−1.82	0.014	0.035	Tags =64%, list =22%, signal =82%
KEGG_RNA_DEGRADATION	59	−0.59	−1.78	0.018	0.045	Tags =47%, list =15%, signal =56%
KEGG_PROTEASOME	46	−0.67	−1.77	0.026	0.046	Tags =63%, list =20%, signal =78%

GSEA, gene set enrichment analysis; KEGG, Kyoto Encyclopedia of Genes and Genomes; ES, enrichment score; NES, normalized enrichment score; NOM, nominal; FDR, false discovery rate.

https://dx.doi.org/10.21037/jgo-22-662